Reduction of Air-Gap Flux Density Distortion for a 20 kW HTS Induction Motor

Masoud Ardestani, Hamid Reza Izadfar

Reduction of Air-Gap Flux Density Distortion for a 20 kW HTS Induction Motor

Masoud Ardestani[1] and Hamid Reza Izadfar[2]

[1] Department of Electrical and Computer Engineering, NOVA School of Science and Technology (FCT NOVA), Caparica, Portugal
[1]ardestani.masoud90@gmail.com
[2] Department of Electrical and Computer Engineering, Semnan University, Semnan, Iran
[2]hrizadfar@semnan.ac.ir

Abstract. Nowadays, High-Temperature Superconducting (HTS) electric machines are widely used in industry due to the unique properties of HTS materials. Besides, the effect of space harmonics is a very serious challenge that must be considered in the design of HTS electric machines. In this paper, a high-temperature superconductor- induction/synchronous machine (HTS-ISM) with 20 kW power is provided to reduce air-gap flux density distortion. For a precise comparison, the main parameters of the machine are studied under the same conditions such as frequency, core material, pole number, critical current density, and voltage by the Finite Element Method. In addition to winding arrangement, the geometrical parameters of the machine also affect the space harmonics, so by modifying each of these parameters, the amount of Total Harmonic Distortion (THD) is obtained in each case. In the proposed model, the amount of THD is significantly reduced, which makes the air-gap flux density more sinusoidal. Torque ripple has also been improved in the proposed machine.

Keywords: High-temperature superconductor, Air-gap flux density, Harmonic component, Total harmonic distortion, Finite element method.

1 Introduction

Today, the development of High-Temperature Superconductor (HTS) machines has increasingly drawn the attention of researchers [1-4]. These types of HTS machines can be used in different applications such as ship propulsion [5], electric vehicles [6], wave energy converters [7], wind energies [8], and so on. However, although superconducting electric machines have been increasingly used in various industries and have unique properties, they are not immune to harmonics, Nevertheless, superconducting machines perform better than conventional machines against harmonic distortion [9]. The problem of harmonics is the main issue in electric machines that must be considered in the design since it affects the performance of electric machines, both superconducting, and conventional machines.

Generally, harmonics are divided into two categories, time, and space harmonics. Time harmonics are caused by nonlinear loads and power electronics devices, but space harmonics are created inside the electric machines. The space harmonics are related to the design, the type of winding (concentrated or distributed), the full or fractional pitch, and the geometry of the machine such as air-gap length, slot opening, eccentricity, and lamination stack, magnetic saturation, etc. [13,14,15]. Apart from that, another issue that must be considered in HTS machines is the design and implementation of HTS coils, which is also effective in reducing the distortion of the air-gap flux density, so that the perpendicular flux to their surface is reduced. Since the anisotropy of HTS coils is completely different from copper winding and their characteristics as critical current density are strongly affected by perpendicular fluxes which leads to a decrease in critical current density, an increase in AC losses, and distortion in the air-gap flux density. Therefore, the proper design of an HTS coil in the superconducting machine is very important to reduce the harmonic component of the air-gap flux density [10,11,12,13,30]. One of these machines discussed in this paper is High-Temperature Superconductor- Induction/Synchronous Machine (HTS-ISM), which is an ideal candidate in the electrical transportation industry. Concerning this, a 20 kW HTS induction motor which was designed and built by Japanese researchers [16] examined from the harmonic perspective. In fact, we analyzed a partial HTS induction motor in which superconducting materials only used in the rotor and stator winding are made of copper exactly like a conventional electric motor [16,19]. On the other hand, since the stator winding was pre-designed as distributed, we have only focused on the motor geometry to reduce the harmonic components in the air-gap. Furthermore, space harmonics in the HTS-ISM cause noise due to the pulsating torque, and increased copper and core losses, which leads to heat and decrease efficiency. For this reason, if the harmonic components of the air-gap can be reduced, the vibration, noise, copper, and core losses of the motor can be decreased [15,20]. Regarding this, the HTS-ISM air-gap magnetic flux distortion is investigated, and a new structure is proposed to reduce the harmonic component of air-gap flux density. For this purpose, the geometric parameters that were effective on the harmonic component of air-gap flux density were investigated and the most appropriate ones were selected from the THD point of view. Also, with decreasing the harmonic components of the air-gap, the torque ripple has decreased. The rest of the paper is as follows. In section 2, the relation of the conference theme with the paper is given. In section 3 the structure of HTS-ISM will be described. In section 4, the HTS-ISM operation is explained. In section 5, the geometry optimization of HTS-ISM is given. In section 6, electromagnetic analysis of the initial and proposed HTS-ISM is investigated. Finally, the conclusion and future work will be explained in sections 7 and 8, respectively.

2 Relation with Technological Innovation for Life Improvement

The technological innovation proposed in this work is related to life improvement by contributing to the development of high-temperature superconducting machines.

Superconducting materials allow the development of more compact and light devices with the same power when compared to their conventional counterparts. This has impacts on several sectors, such as industry or transportation. The development of superconducting-based technologies has also direct impact on life improvement, as related to all the links of the energy chain, besides end-use, like generation, transmission, distribution, and storage of electrical energy, fostering the Energy Transition.

3 Machine Structure

The initial machine structure is shown in Fig. 1[16]. The stator and rotor cores are silicon-steel and laminated. The stator coil is made of copper and the distributed winding is adopted to reduce the harmonic component of the air-gap magnetic flux density [17]. Also, rotor bars with HTS wires (Bi-2223) are located in the rotor slots. Since the core of the motor passes almost all of the main magnetic flux from the slots, it has two major advantages over the air-core motor: 1- There are only self-magnetic fields in the slots i.e., magnetic field leakage due to the current passing through the HTS rotor bars, in other words, there is no external magnetic field in the rotor bars. Therefore, the destructive effects of magnetic fields on the current transport property can be ignored. 2- Reducing the electromagnetic force applied on rotor HTS bars, therefore does not need a complex structure to protect the conductors [26]. The HTS rotor bars are mounted on the top of the rotor near the air-gap to reduce leakage flux [27].

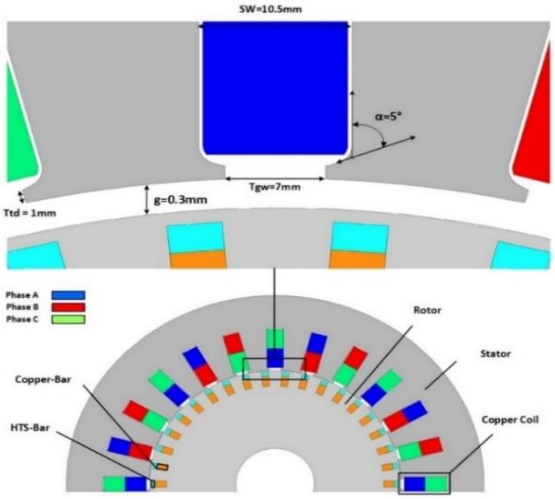

Fig.1. The structure of the initial machine

Rotor bars are made of eleven HTS tapes, isolated copper bars are also used in the rotor slots for thermal stability, mechanical support, and current pass in the non-superconducting area of the HTS bars [18]. At the time of starting, the motor has to be cooled to 77 k. The length of the cryostat is the length of the shaft with a diameter of 428 mm. The cryostat structure is such that the HTS-ISM can rotate slowly even below the Cryogenic temperature and the cryostat is equipped with a nitrogen reservoir [16]. Since the stator and rotor cores are laminated, the effects of eddy losses are neglected. All the analyses of the proposed and initial machines were carried out under the identical conditions such as the coil number, speed, core materials, and poles number. The specification of HTS wire and the main parameter of the HTS-ISM are presented in Table 1 and Table 2, respectively.

Table 1. Specification of HTS wire

HTS wire	**Type H**
Width	4.3±0.3 mm
Thickness	0.23±0.23 mm
I_C at 77 k, self-field	190 A
Allowable banding radius	70 mm

Table 2. Main parameter of HTS-ISM

Item	**Basic HTS-ISM**
Rated Power	20 kW
Rated speed	750 Rpm
frequency	50 Hz
Number of poles	8
Air-gap	0.3mm
Stator number of coils turns	30
Critical current of rotor winding	2090 A
materials of stator winding	Copper
materials of rotor winding	DI-BSCCO Type H
inner diameter of stator	160mm
outer diameter of stator	256mm
inner diameter of rotor	50mm
outer diameter of rotor	159.4mm
rotor slot number	38
stator slot number	24

4 Machine Operation

When AC voltage is applied to an HTS induction motor, the rotor bars are exposed to time-varying magnetic flux due to the MMF caused by the stator winding. On the other hand, since the rotor bars are made of high-temperature superconducting material and type Bi-2223, they show losses against AC fields. Also, another type of loss due to thermal activation occurs in currents below J_c, called Flux creep. In addition, superconducting materials have inherent properties and impurities, so their interaction with time-varying magnetic fields creates a force called the pinning force.

This force keeps in place the vortices that cause losses in superconducting materials. At the opposite point, there is another force called the Lorenz force that wants to move the vortices. When these two forces are equal, that point is the critical current density. Thus, in the initial moments, since the motor has not yet started to rotate and the magnetic field applied to the rotor bars is less than Hc_1, the flux applied to the rotor bars is shielded because of pinning centers and they are not allowed to enter the bars, which this is called initial mode (shielding). At this moment, the magnetic flux inside the rotor bars is zero (B = 0). After a while, as the motor starts to rotate due to high slip (s = 1), high currents are created in the rotor bars. In this situation, the Lorenz force is greater than the pinning force, which causes the vortices to flow in the rotor bars, and the bars show resistance losses, which is called Flux-Flow or Asynchronous mode. At this moment, rotor bars current also greater than the critical current density of the bars, which is 2090 amps, so the bars are out of superconductivity for a short time. In this case, the motor starts with a slip, which is obtained as follows (1).

$$S = \frac{N_S - N}{N_S} \tag{1}$$

Where, N_s is the synchronous speed and N_r is the speed of rotor. Moments later, due to the reduction of slip, the current of the rotor bars becomes less than the critical current density of the bars and the resistance of the rotor bars becomes almost zero. At this time, the Lorentz force is less than the pinning force, and all magnetic flux is trapped by the pinning centers in the rotor bars, which is called persistent current mode or Synchronous mode. At this time, the rotor is locked with a magnetic field and reaches synchronous speed. In this case, the rotor bars act like PM. In fact, this motor has 3 modes of shielding, asynchronous and synchronous due to the unique properties of superconducting materials that have nonlinear resistance. This nonlinear resistance leads the motor to have high starting torque (due to high resistance) and synchronous torque (due to almost zero resistance) [17,21,24,27,33].

4.1 The Relationship between Voltage-Current of Superconductor and Torque-Speed of HTS-ISM

To use a superconductor, its electromagnetic behavior must be described. Quantitative calculation of the electromagnetic behavior of HTS materials is complex because their voltage-current relationship is non-linear. The E-j power-law method uses the nonlinear

voltage-current superconductor relation to model it as a nonlinear conductor. The voltage-current curve of the superconductor and torque-speed of HTS-ISM is shown in Fig 2. the superconductor voltage-current curve can be fit by the power-law given in Equation 2.

$$E(I) = E_C\left(\frac{I}{I_C}\right)^N \tag{2}$$

Where E(I) is the longitudinal voltage drop through the superconductor, EC is the electric field criterion at 1μv/cm, I is the current in the conductor, IC is the critical current, and N is the exponent. A higher N-value produces a sharp transition in the V-I curve and demonstrates the quality of the superconductor. High-quality superconductors will have numerous N-value. A superconductor is categorized by a V-I curve or the voltage drop across the length of it as a function of its current. The critical current of the superconductor is defined as the current that produces a voltage drop of 1 μv/cm as depicted in Fig. 2. According to Fig.2., this motor not only has a slip torque but also synchronous torque. In simple terms, the rotational synchronous mode is achieved in zero resistivity state and rotational slip mode is achieved in the flux-flow state. These exclusive features are due to the nonlinear voltage current of HTS materials [9,25].

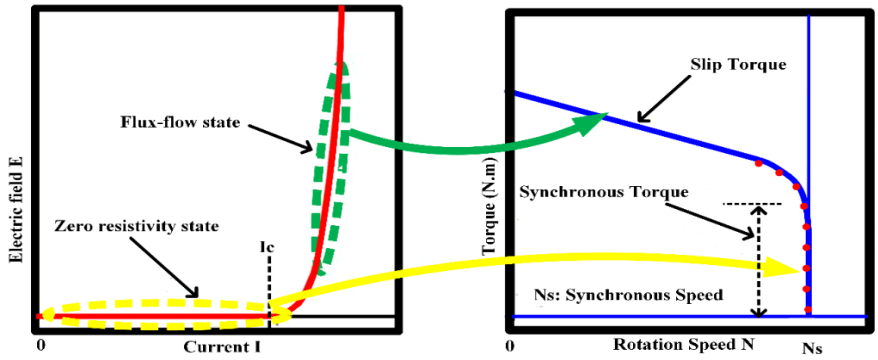

Fig.2. The voltage-current of superconductor relationship with torque-speed of HTS-ISM [25].

5 Motor Geometry Optimization

Generally, in an electric machine, the geometrical parameters of the machine and the structure of the winding affect the space harmonics. So, by choosing these parameters properly, the effects of the space harmonics, which result in vibration, parasitic torque, noise, and losses, can be reduced. In this section we only focused on the geometrical parameters of the motor because the winding arrangement of the initial motor has been designed as distributed with a short pitch configuration. Therefore, to investigate the air-gap magnetic flux density in terms of harmonic, first, air-gap magnetic flux density was acquired based on FEM with the ANSYS-Maxwell software. After that, the Fourier

transform was obtained from the air-gap magnetic flux by MATLAB software, and the THD value of air-gap flux was attained for each variable which is presented in Fig. 4. The parameters examined are air-gap (g), tooth gap width (Tgw), slot width (Sw), tooth tang angle (α), and tooth tang depth (Ttd) as shown in Fig. 3. Fig. 4 (a) shows the rate of THD changes of parameters which their unit is length (air-gap, tooth gap width, slot width, tooth tang depth). Fig. 4 (b) also shows the THD value of tooth tang angle parameter for different angles in degree. In addition, an explanation of all the examined parameters is given below. Finally, the THD values for different parameters are given in Table 3.

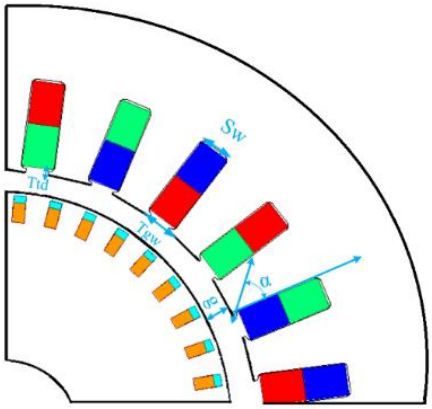

Fig.3. Examined parameters of HTS-ISM.

5.1 Air-gap

Air-gap is the most important factor in reducing air-gap magnetic flux density distortion. The length of the air-gap of the initial HTS-ISM is 0.3 mm. By increasing this parameter from 0.3 to 1 mm, the odd harmonics components of the air-gap magnetic flux decreased, the reason behind this, is the variation of permeance which affects the amplitude of the harmonic component [20]. Also, the amplitude of the fundamental component is reduced due to the increase in the air-gap magnetic reluctance. The lowest value of THD belongs to the air-gap of 1 mm.

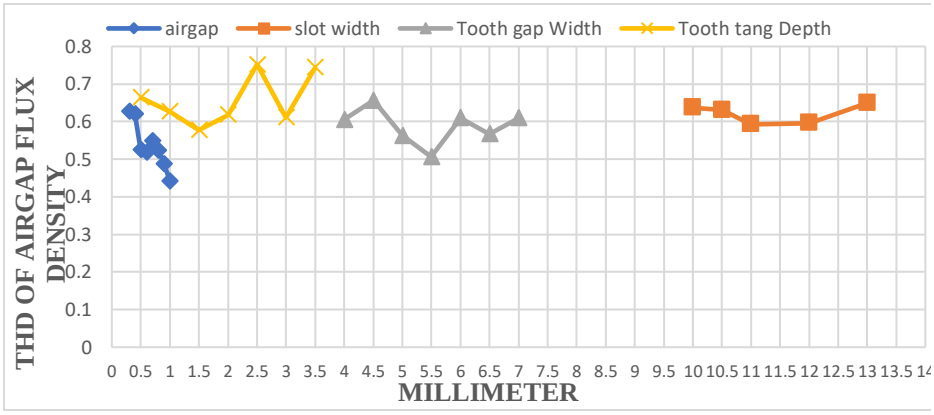

(a)

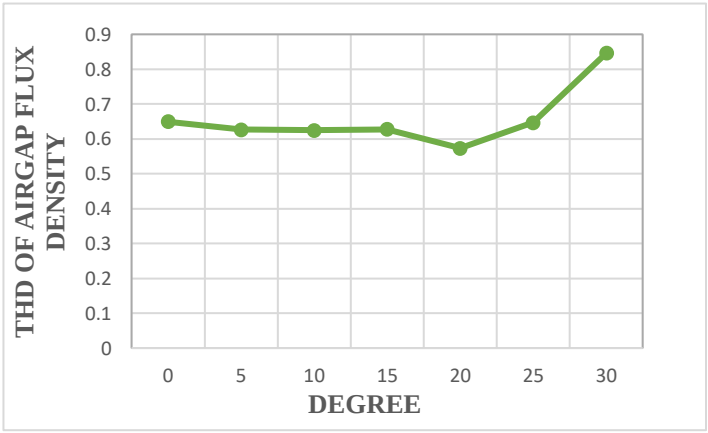

(b)

Fig.4. The THD values for different parameters a) parameters with different unit lengths b) Tooth tang angle parameter with unit of degree.

5.2 Tooth Gap Width

After the air-gap, the gap between the teeth which is called tooth gap width is the most important parameter in reducing THD of the air-gap magnetic flux. By changing this parameter to 5.5 mm, the THD reaches its minimum value which is 0.5064.

5.3 Slot Width

The slot width is designed according to machine limitations such as specific magnetic loading and specific electric loading. As the slot width increases, the specific electric loading increases, and by decreasing it, the specific magnetic loading increases. Therefore, the slot width should be selected according to the limitations of the machine such as the standard current density in the stator coil and the maximum allowable magnetic flux density; regarding the need and the limitations of the machine, a compromise should be made between the specific magnetic loading and specific electric loading. To optimally select the dimensions of the slot, equation 3 must be satisfied.

$$A_{SS} = \frac{Z_{SS} a_S}{0.4} \tag{3}$$

Where Z_{SS} is the number of conductors, a_S is the conductor cross-section, 0.4 is a constant coefficient and A_{SS} is the slot area. By varying the slot width from 10 to 13 mm, the THD value of the air-gap flux belongs to the slot width of 11 mm with a value of 0.5927.

5.4 Tooth Tang Angle

The tooth tang angle is the angle between the tang and the bottom of the slot. The variation of the THD of tooth tang angle changes in terms of degree is shown in Fig. 4 (b), the lowest of which is at 20 °.

5.5 Tooth Tang Depth

Tooth tang depth is the length of the tang. The lowest THD value of the air-gap belongs to the tooth tang depth of 1.5 mm. As shown in Table 3, the minimum THD values for the examined parameters (air-gap, tooth gap width, slot width, tooth tang angle, and tooth tang depth) are 1mm, 5.5 mm, 11 mm, 20˚, and 1.5 mm respectively. Therefore, the proposed machine is designed with these values.

Table 3. THD values for the examined machine parameters in different range.

Examined Parameter	Examined parameter variation	THD of Air-gap Flux Density
Air-gap (mm)	0.3	0.6267
	0.4	0.6209
	0.5	0.5252
	0.6	0.5183
	0.7	0.5496
	0.8	0.5229
	0.9	0.4869
	1	0.4415
Tooth gap width (mm)	4	0.6052
	4.5	0.6566
	5	0.5633
	5.5	0.5063
	6	0.61
	6.5	0.5668
	7	0.6096
Slot width (mm)	10	0.6372
	10.5	0.631
	11	0.5927
	12	0.5958
	13	0.6494
Tooth tang angle (degree)	0	0.65
	5	0.6267
	10	0.6249
	15	0.6277
	20	0.5736
	25	0.647
	30	0.8456
Tooth tang depth (mm)	0.5	0.6643
	1	0.6267
	1.5	0.5774
	2	0.6184
	2.5	0.7522
	3	0.6111
	3.5	0.7439

6 2D FEM Analysis

Analytical equations cannot be used when the geometry is complicated, and the field

condition is not uniform. Numerous numerical methods have been proposed to solve this problem. These numerical methods usually use the FEM and FDM methods to solve the Maxwell equations. FEM is the most popular method for solving partial differential equations. These methods can be categorized by solving the Maxwell equations that are the same: A-V (based on the magnetic vector potential A), T- Ω (based on the current vector potential T), E (based on the electric field E), and H (based on directly solving the magnetic field components) formulations. The final answer to each of these equations is the same.; the only difference is their solutions [27-29]. The numerical model used in this paper for modeling of HTS-ISM is based on solving the set of Maxwell equations in 2D implementing the A-V formulation using the software package ANSYS-Maxwell. Therefore, by solving the partial differential equation (PDE) in 2D, the amount of electric and magnetic fields in each node can be accurately obtained from the equation (4).

$$\nabla \times \upsilon \nabla \times A = J_S - \sigma \frac{dA}{dt} - \sigma \nabla v + \nabla \times H_C \tag{4}$$

Where A is the magnetic vector potential, J_s is the source current density (one component in z-direction for 2D), H_C is the coercive magnetic field (A/m) and v is the velocity of the moving part. For a simple definition of the HTS materials, a material called perfect conductor which also exist in the ANSYS-Maxwell Library, is included with a magnetic relative permeability of almost zero.

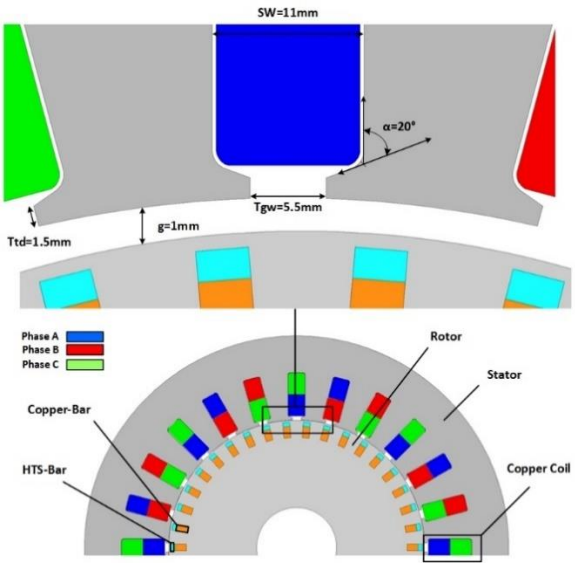

Fig.5. The structure of the proposed machine.

The proposed machine is designed based on the initial machine as shown in Fig. 5. According to the results of the previous section, the lowest THD values were obtained by

changing air-gap, tooth gap width, slot width, tooth tang angle, and tooth tang depth values by 1mm, 5.5mm, 11mm, 20˚ degree, and 1.5mm, respectively. In this section, the electromagnetic parameters of the initial and proposed machine are presented and investigated, such as the distribution of the air-gap magnetic flux and its harmonic components, magnetic flux lines and magnetic flux density distribution, and torque ripple.

6.1 Air-gap Flux Density Distribution and Harmonic Component

The interaction between the stator and the rotor MMF leads to magnetic flux density in the air-gap of the HTS induction motor. So that the voltage applied to the stator winding, which causes induced current in the cage rotor, creates MMF in the stator and rotor winding, respectively. Space harmonics make the air-gap magnetic flux distorted, so it is not purely sinusoidal. To detect the decrease and increase of air-gap magnetic flux density harmonics, Fourier transforms which are known as the total harmonic distortion (THD) criterion, could be utilized. Generally, the THD relation in terms of air-gap magnetic radial flux (Br) can be defined as below. The tangential flux is ignored.

$$THD = \frac{\sqrt{\sum_{k=2} Brk^2}}{Br1} \tag{5}$$

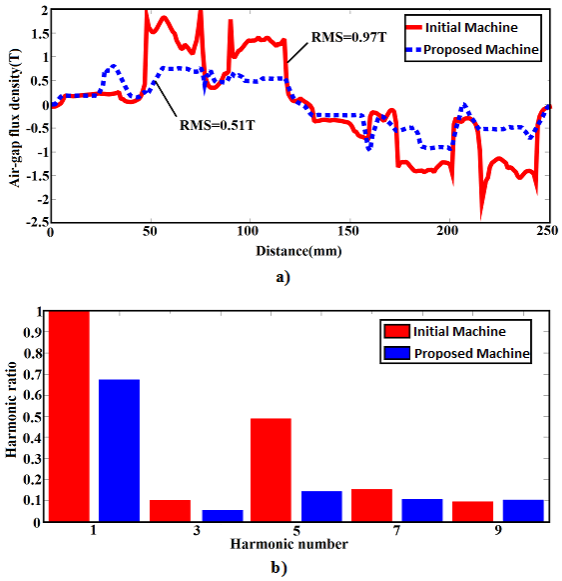

Fig.6. Air-gap flux density a) air-gap flux density distribution b) air-gap flux density harmonic component.

Where k is an integer and refers to harmonics (k = 1,2,3,4, ...), B_{rk} is the K_{th} amplitude of the K_{th} order harmonic and B_{r1} is the fundamental component [26,30]. pursuant to equation (5), the lower the amplitude of the harmonic components, the lower the THD, and the waveform gets closer to the main component, which is a pure sine wave. The distribution of air-gap flux density is shown in Fig. 6 (a). As can be seen, the RMS value of air-gap flux density in the proposed machine is lower than the initial one, and that is the main disadvantage of air-gap increases which leads to reducing the air-gap magnetic flux magnitude. On the other hand, by reducing the air-gap distance the harmonic ratio also decreases significantly. Fig. 6 (b) shows the odd harmonic components of the initial and the proposed machines. As shown in Fig. 6 (b), the amplitude of components 3, 5, and 7th decreased, which made the magnetic flux of the air-gap more sinusoidal. Also, the amplitude of the first component, which is the fundamental component is reduced due to the elimination of space disturbing harmonic components. The obtained amount of THD in the proposed machine was 0.4126 and in the initial machine was 0.6267 under 112 Nm load, which was reduced by 34.17% in the proposed machine.

6.2 Magnetic Flux Density Distribution and Magnetic Flux Lines

Fig. 7 shows the distribution and flux line density of magnetic flux in the stator and rotor of the initial and proposed machine under a load of 112 Nm. As can be seen from the figure, the magnetic flux density distribution is higher in the initial machine due to the smaller air-gap of the initial machine compared to the proposed machine. On the other hand, since the analysis of both machines was performed under the same conditions, the applied voltage to both machines was equal, which caused a small saturation in the stator teeth of the initial machine. In general, increasing the air-gap increases the magnetizing current of the motor, which causes the motor to draw more current from the grid, so it needs to apply more voltage. The maximum magnetic flux density is set at 2.5 tesla, which is less than 2.5 tesla in both machines. Besides, the flux line intensities in the proposed machine are weaker than the initial machine due to the increase in air-gap [31].

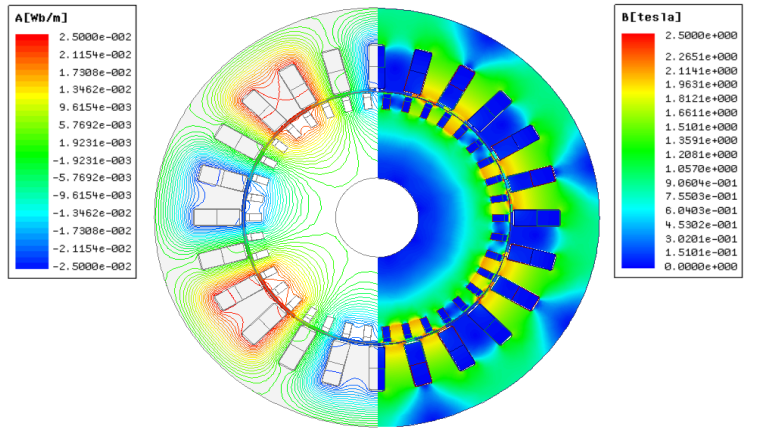

a)

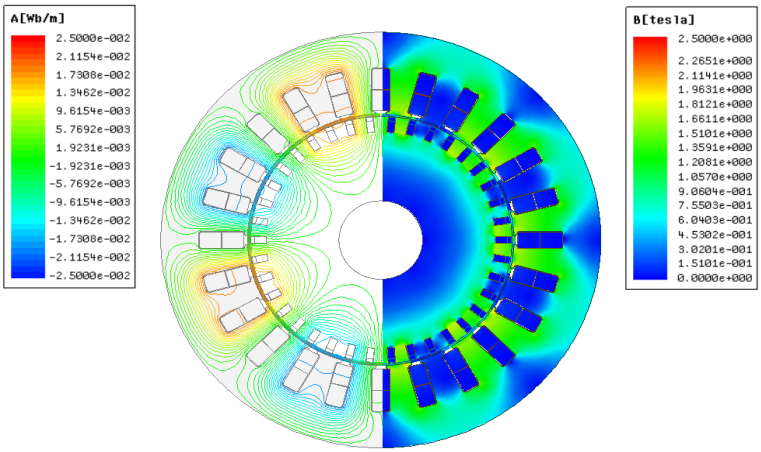

b)

Fig.7. Magnetic flux lines and magnetic flux density distribution a) initial machine b) proposed machine.

6.3 Torque Ripple

Torque ripple is one of the effects that can be observed in the majority of motors and the reason is the periodical increment and reduction of the output torque in the motor shaft. The amount of torque is often expressed as a percentage, which can be calculated by the

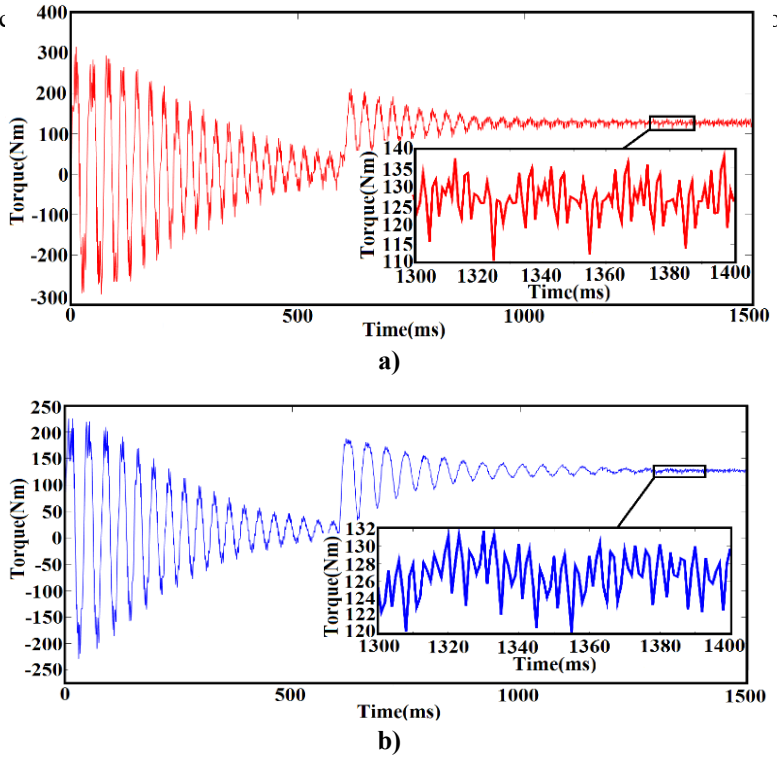

Fig.8. Transient curve of torque. a) initial machine. b) proposed machine.

difference between the maximum and minimum electromagnetic torques to their average over a period, using the following relation:

$$\text{Torque ripple} = \frac{T_{max} - T_{min}}{T_{avg}} \times 100 \quad (6)$$

Where, T_{max} is the maximum torque, T_{min} is the minimum torque and T_{ave} is the average torque [36]. Based on Fig. 8, when the motor is in synchronous speed and in steady state, a load equal to maximum synchronous torque (112 Nm) which was measured in [16] is applied to the motor shaft at the time of 0.6 seconds. The motor power, in this case, is about 8.7 kW. In Fig. 8 (a), at 1.3 to 1.4 seconds (s), the maximum torque and the minimum torque, and average torque are 137.95, 110.79, and 124.37 respectively. Fig. 8 (b) shows the maximum torque of 131.77 and minimum torque of 120.11 and a mean torque of 125.94 at 1.3 and 1.4 seconds, respectively. So that the torque ripple is 9.2% in the proposed machine and 21.8% in the initial machine. As can be seen from Fig. 8, the torque ripple in the proposed machine is 12.6% lower than in the initial machine.

7 Conclusions

In this paper, a 20 kW HTS induction motor with the new physical model is presented to reduce the air-gap flux density distortion. The cause of distortion in the air-gap flux density of electric machines is related to space harmonics. These harmonics can be reduced or eliminated by a modification of the winding configuration and motor geometry. Concerning this, we only focused on motor geometry parameters, since the stator winding was predesigned as distributed with a short pitch factor. The geometrical parameters which we investigated were air-gap, tooth gap width, slot width, tooth tang depth, and tooth tang angle, respectively. So that, by changing each of these parameters and selecting the best ones, the optimal model of the machine is obtained from the harmonic point of view. In addition, the most important parameter that reduced the harmonic component of the air-gap flux density was the air-gap changes. Also, all analyses were performed under the same conditions such as voltage, current, pole number, current density, etc. by ANSYS-Maxwell software. Eventually, In the proposed model, THD decreases from 0.6267 to 0.4126 with a decrease of 34.17%. Torque ripple has also decreased from 21.8% to 9.2% by a 12.6% decrease, which results in improving the performance of the machine.

8 Future Work

This HTS motor has been improved by Japanese researchers for many years. Besides, this motor was made in two types of partial and fully HTS induction motors. In the partial structure, HTS materials are used in the rotor, and copper is used only in the stator windings, but in the fully structure, HTS materials are used in both the stator and the rotor. This approach, which is used in this paper to reduce the harmonic component of air-gap flux density, has the potential to be implemented in other structures of HTS induction motors such as fully HTS induction motors or higher power HTS induction motors with both structures (partial and fully) which also built-in recent years. Although in general all parameters must be considered for the design of electric motors and compromise between the parameters is necessary, nevertheless, this approach, regardless of its disadvantages, is a good candidate to reduce the harmonic component of air-gap flux density.

References

[1] K. Umemoto, K. Aizawa, M. Yokoyama, K. Yoshikawa, Y. Kimura, M. Izumi, K. Ohashi, M. Numano, K. Okumura, M. Yamaguchi, Y. Gocho, E. Kosuge, Development of 1 MW-class HTS motor for podded ship propulsion system, in: J. Phys. Conf. 234, Ser (2010)

[2] B. Gamble, G. Snitchler, T. Macdonald, Full power test of a 36.5 MW HTS propulsion motor, IEEE Transactions on Applied Superconductivity. 21, 1083-1088 (2011)

[3] E. Ueno, T. Kato, K. Hayashi, Race-track coils for a 3 MW HTS ship motor, Physica C:

Superconductivity and Its Applications. 504, 111-114 (2014)
[4] Z. Huang, W. Xian, M. Zhang, M. Chudy, Y. Chen, Z. Zhong, M. Baghdadi, W. Wang, F. Spaven, K. Matsuda, T.A. Coombs, Control and operation of a high temperature superconducting synchronous motor, IEEE Transactions on Applied Superconductivity. 3, 235200204-5200204 (2013)
[5] G. Snitchler, B. Gamble, S.S. Kalsi, The performance of a 5 MW high temperature superconductor ship propulsion motor, IEEE Transactions on Applied Superconductivity. 15, 2206–2209 (2005)
[6] T. Karashima, T. Nakamura, M. Okuno, Multidisciplinary analysis of the transient performance of a 20 kW class HTS induction / synchronous motor cooled with a cryocooler and gaseous air-gap coolant. Elsevier, Cryogenics. 99, 9961–67 (2019)
[7] M. Ardestani, N. Arish, H. Yaghobi, A new HTS dual stator linear permanent magnet Vernier machine with Halbach array for wave energy conversion, Physica C: Superconductivity and Its Applications. 569, 1353593 (2020)
[8] B.S. Go, H.J. Sung, M. Park, I.K. Yu, Structural design of a module coil for a 12-MW class HTS generator for wind turbine, IEEE Transactions on Applied Superconductivity. 27, 1-5 (2017)
[9] Swarn Singh Kalsi, Applications of High Temperature Superconductors to Electric Power Equipment, Wiley &Sons (2011)
[10] K. Ikeda et al., DC and AC Current Transport Characteristics of the HTS Stator Coils in an HTS Induction/Synchronous Motor, IEEE Trans. Appl.supercond. Supercond.,28 (3),14–18 (2018)
[11] M. Yazdani-Asrami, S. Asghar Gholamian, S. M. Mirimani, and J. Adabi, Influence of field-dependent critical current on harmonic AC loss analysis in HTS coils for superconducting transformers supplying non-linear loads, *Cryogenics.*,113, 103234 (2021)
[12] L. Wei, T. Nakamura, M. Yoshikawa, Y. Itoh, and T. Terazawa, Comparison of Different Stator Winding Configurations of Fully High-Temperature Superconducting Induction/Synchronous Motor, *IEEE Trans. Appl. Supercond.*, 30 (4), 4–7 (2020)
[13] B. Lukasik, K. F. Goddard and J. K. Sykulski, Finite element assisted method to reduce harmonic content in the airgap flux density of a high temperature superconducting coreless rotor generator, *2008 IET 7th International Conference on Computation in Electromagnetics*, 56-57 (2008)
[14] G.N. On, Guidance Note to Control of Harmonics in Electrical Power Systems, American Bureau Of shipping ABS plaza 16855 Northchase Drive Houston, TX 77060 USA (2006)
[15] G.J. Wakileh, Harmonics in rotating machines, Electric Power System Research. 66, 31– 37 (2003)
[16] D. Sekiguchi, T. Nakamura, S. Misawa, H. Kitano, T. Matsuo, N. Amemiya, Y. Ito, M. Yoshikawa, T. Terazawa, K. Osamura, Y. Ohashi, N. Okumura, Trial test of fully HTS induction/synchronous machine for next generation electric vehicle, IEEE Transactions on Applied Superconductivity. 22, 5200904-5200904 (2012)
[17] T. Karashima, T. Nakamura, K. Ikeda, N. Amemiya, M. Yoshikawa, Y. Itoh, T. Terazawa, Y. Ohashi, Experimental and analytical studies on highly efficient regenerative characteristics of a 20-kW class HTS induction/synchronous motor, IEEE Transactions on Applied Superconductivity. 27, 1-5 (2017)
[18] H. Shimura, T. Nakamura, H. Kitano, T. Nishimura, N. Amemiya, Y. Itoh, Calculated characteristics of HTS induction/synchronous machine below and above its critical temperature, IEEE Transactions on Applied Superconductivity. 23, 5201705-5201705 (2013)
[19] M. Ardestani, H. Hefaz, N. Arish, H. Yaghobi, Electromagnetic Analysis of Partial and Fully

HTS Induction Motor Using Finite Element Method, 28th Iranian Conference on Electrical Engineering (ICEE), pp. 1-5, Tabriz, Iran. (2020)
[20] J.A. Cordier, Modelling space harmonics in induction machines for real-time applications, PhD Thesis Technical university of munich, (2020)
[21] G. Morita, T. Nakamura, I. Muta, Theoretical analysis of a YBCO squirrel-cage type induction motor based on an equivalent circuit, Supercond. Sci. Technol. 19, 473–478 (2006)
[22] T. Nakamura, H. Miyake, Y. Ogama, G. Morita, I. Muta, T. Hoshino, Fabrication and characteristics of HTS induction motor by the use of Bi-2223/Ag squirrel-cage rotor, IEEE Transactions on Applied Superconductivity. 16, 1469–1472 (2006)
[23] G. Morita, T. Nakamura, I. Muta, Theoretical analysis of a YBCO squirrel-cage type induction motor based on an equivalent circuit, Supercond. Sci. Technol. 19, 473–478 (2006)
[24] M,Murakami, Magnetic properties of high temperature superconductor, IEEE Transactions on Applied Superconductivity. 8, 405-414 (1993)
[25] K. Ikeda, T. Nakamura, T. Karashima, N. Amemiya, M. Yoshikawa, Y. Itoh, T. Terazawa, Y. Ohashi, Hysteretic rotating characteristics of an HTS induction/synchronous motor, IEEE Transactions on Applied Superconductivity. 27, 1-5 (2017)
[26] J. Laksar, J. Sobra, L.Veg, Numerical Calculation of the Effect of the Induction Machine Load on the Air Gap Magnetic Flux Density Distribution, 18th International Scientific Conference on Electric Power Engineering (EPE). 1-6 (2017)
[27] M. Ainslie, Transport AC loss in high-temperature superconducting coils, Ph.D. Thesis, University of Cambridge; (2012)
[28] M.Y.S. Asghar, G. Seyyed, M. Mirimani, J. Adabi, Calculation of AC Magnetizing Loss of ReBCO Superconducting Tapes Subjected to Applied Distorted Magnetic Fields, J. Supercond. Nov. Magn. 31, 3875–3888 (2018)
[29] L. Wang, J. Zheng, F. Jiang, R. Kang, Numerical Simulation of AC Loss in 2G High-Temperature Superconducting Coils with 2D-Axisymmetric Finite Element Model by Magnetic Field Formulation Module, J. Supercond. Nov. Magn. 29, 2011-2018 (2016)
[30] R. Kulkarni, K. Prasad, T.T. Lie, R.A. Badcock, C.W. Bumby, H.J. Sung, Design improvisation for reduced harmonic distortion in a flux pump-integrated HTS generator, Energies. 10(9), 1344 (2017)
[31] Q. Chen, G. Liu, Z. Liu, X. Li, Design and Analysis of a New Fully Stator-HTS Motor, IEEE Transactions on Applied Superconductivity. 24, 1-5 (2014)
[32] B. Liu, R. Badcock, H. Shu, L. Tan, J. Fang, Electromagnetic Characteristic Analysis and Optimization Design of a Novel HTS Coreless Induction Motor For High-Speed Operation, IEEE Transactions on Applied Superconductivity. 28, 1-5 (2018)
[33] N. Arish, M. Ardestani, A Hekmati, Optimum structure of rotor slot for a 20 kW HTS Induction motor, Physica C: Superconductivity and Its Applications. 582, 1353829 (2021)